Analysis of off-axis performance of compliant mechanisms with applications to mobile millirobot design

A. M. Hoover and R. S. Fearing

Abstract— **We present an approach to quantifying the off-axis stiffness properties of parallel compliant mechanisms used in the design of mobile millirobots. By transforming the stiffness of individual flexure elements and rigid links comprising a compliant mechanism into a global coordinate system, we enable the formulation of an equivalent mechanism stiffness. Using that stiffness in concert with an energy-based performance metric, we predict the performance of a compliant mechanism subjected to a prescribed set of forces in the global coordinate system. We analyze a flexure-based Sarrus linkage and use the performance metric to improve the design by adding topological redundancy. Finally, our approach is experimentally validated by constructing and testing SCM Sarrus linkages in a variety of geometries and topologies and demonstrating agreement between the model and our experiments.**

I. INTRODUCTION

Compliant mechanisms are a useful class of mechanisms because they attain their mobility from the elastic deformation of compliant members. The term "compliant mechanism" has been broadly used in the literature to describe both continuum mechanisms in which large scale deformation can be distributed throughout the body [21] [16] and so-called discrete or lumped compliance models in which compliance is concentrated at nodes which are connected using members that are generally assumed to be rigid [13] [12]. Because they have no moving parts, they are free from backlash and friction, require no lubrication, and are suitable for use at the microscale. These advantages have led to their adoption in a variety of robotic applications from microscale silicon-based robots [4] [9], to high resolution mesoscale precision positioning devices [1] [3], to milliscale mobile robots with microscale feature sizes [17] [11] as well as scaled prototypes of such robots [10].

The most typical approach to design and modeling of compliant mechanisms is the finite element method (FEM) in which the body is subdivided into mesh elements and a large system of equations relating the tractions to the displacements for each elastic element are solved numerically. This method can be very powerful for optimizing or predicting the behavior of an existing topology [8], but its complexity and lack of analytical predictive power make it a cumbersome tool to apply during initial design or prototyping stages.

The work was supported by the Army Research Laboratory under the Micro Autonomous Science and Technology Collaborative Technology Alliance

A. M. Hoover is with the Department of Mechanical Engineering, University of California, Berkeley ahoover@eecs.berkeley.edu

R. S. Fearing is faculty in the Department of Electrical Engineering and Computer Science, University of California, Berkeley ronf@eecs.berkeley.edu

By contrast, Howell's pseudo-rigid-body model (PRBM) [12] was developed in an effort to simplify the compliant mechanism design process and bridge the gap between rigid mechanism design and compliant mechanism design. The PRBM models compliant mechanisms as rigid body members connected by ideal pin joint hinges in parallel with torsional springs. The resulting mechanisms have force(moment)/displacement curves approximately equivalent to their compliant analogs and enable accurate analysis that includes large displacements. The primary limitation of the PRBM is the ideal pin joint behavior assumption. The idealization of simple flexures as pin joints with parallel torsional springs reduces the analysis at each joint to a single degree of freedom problem. In practice, flexures experience loading and the consequent displacements in as many six axes. For larger scale devices or mechanisms where the applied and reaction loads are consistent and predictable this limitation of the PRBM may not be significant. However, for small scale mechanisms incorporated into millirobots where actuation involves the amplification of very small strains [19], the consideration of additional off-axis loads and displacements becomes increasingly important for avoiding the loss of actuator displacement to serial compliance in the structure.

In cases where we are willing to assume small deflections, we may explicitly incorporate these effects (in closed form) into our model in order to better study the off-axis behavior of a mechanism. In this work, we address the problem of improving the design of a single degree of freedom (DOF) compliant mechanism consisting of rigid links connected by simple flat (or blade) flexure hinges experiencing small deflections. Specifically, we are interested in improving the various off-axis stiffnesses of such mechanisms while preserving the output motion in the desired direction. Motivation for studying this problem comes from our experience designing and building millimeter scale robots (millirobots) using an approach that integrates rigid composite fiber beams with flat polymer flexure hinges [18]. The example mechanism to which we apply our analysis here is the compliant version of a simple 1 DOF exact straight line linkage known as the Sarrus linkage after its inventor, French mathematician Pierre Frédéric Sarrus.

We begin by reviewing the full 6x6 compliance matrix of a simple flexure in a local coordinate system creating the basis for analyzing more complex combinations of rigid links and flexure hinges. Using the mechanism geometry, the compliance of each individual flexure is transformed into a common coordinate system following the method described in [6]

and [7]. This approach enables the closed form analysis of an equivalent compliance/stiffness for the entire mechanism. Following the exposition of the compliance transformation technique, we propose the use of a strain energy-based metric by which to judge the fitness of a design. Using that metric, we explore and characterize different topologies and geometries for the compliant Sarrus linkage. Finally, results are validated with measurements of representative compliant mechanisms.

II. Modeling Mechanism Stiffness

The approach described below follows the generalized flexure mechanism analysis outlined in [6]. Aside from the linear elasticity assumptions made in formulating the compliance for a single flexure, the primary underlying principle is that a compliant mechanism comprised of flexures and rigid bodies can be modeled as a network of springs. Each flexure is modeled in a local coordinate system as a spring with a 6x6 compliance matrix, $\mathbf{C}$, the inverse of which is its stiffness matrix, $\mathbf{K}$. Then using the mechanism's geometry (eg. link lengths, angles, etc.) and topology (eg parallel or serial chains, number of chains, etc) the individual compliances can be transformed into a common coordinate system and combined appropriately to yield an overall mechanisms stiffness.

A. Compliance of a Simple Beam Flexure

In order to model the equivalent stiffness of a parallel flexure mechanism, it's necessary to formulate the compliance matrix for a single flexure. The end of a single flexure possesses six degrees of freedom with respect to the base - three linear displacements and three angular displacements. Thus, we can construct a matrix relating the displacements at a given point along the length of the flexure to the applied loads. If the generalized load is represented as a six dimensional vector of three forces and three torques, the six dimensional displacement vector will be represented by three differential linear and three differential angular displacements. The matrix that relates generalized forces (or wrenches) to these displacements is called the compliance matrix.

It has been demonstrated in [6] and [14] that it's possible (and useful) to choose a local coordinate system that diagonalizes the compliance matrix of a beam-type flexure. In other words, a local coordinate system can be chosen so that there is no coupling between any of the six degrees of freedom of the flexure. Fig. 1 depicts such a coordinate system located at the intersection of the principal axes of the beam.

The 6x6 compliance matrix of the beam is given by the following equations:

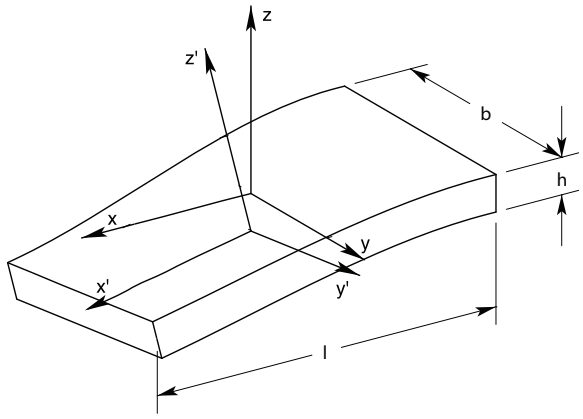

Fig. 1. From [6]: A flat flexure depicting local coordinate systems before $(\mathbf{x}, \mathbf{y}, \mathbf{z})$ and after $(\mathbf{x}', \mathbf{y}', \mathbf{z}')$ deformation. This choice of local coordinate system diagonalizes the compliance matrix.

$$C = \begin{bmatrix} C_x & 0 & 0 & 0 & 0 & 0 \\ 0 & C_y & 0 & 0 & 0 & 0 \\ 0 & 0 & C_z & 0 & 0 & 0 \\ 0 & 0 & 0 & C_{\theta_x} & 0 & 0 \\ 0 & 0 & 0 & 0 & C_{\theta_y} & 0 \\ 0 & 0 & 0 & 0 & 0 & C_{\theta_z} \end{bmatrix} \tag{1}$$

where

$$C_x = \frac{l}{Ehb} \tag{2}$$

$$C_y = \frac{l^3}{Ehb^3} + \frac{2.4l(1+\nu)}{Ebh} \tag{3}$$

$$C_z \approx \frac{l^3}{Ebh^3}\left[1 - \frac{6}{5}\gamma + \frac{17}{35}\gamma^2 - \frac{62}{315}\gamma^3\right] + \frac{2.4l(1+\nu)}{Ebh} \tag{4}$$

$$C_{\theta_x} = 12\left[\frac{1}{2(1+\nu)}\left(4 + 2.52\frac{h}{b}\right)\frac{Ebh^3}{l} + \frac{b^2}{C_z}\right]^{-1} \tag{5}$$

$$C_{\theta_y} = \frac{12l}{Ebh^3}\left[1 + 2\gamma + \frac{6}{5}\gamma^2 + \frac{12}{35}\gamma^3\right] \tag{6}$$

$$C_{\theta_z} = \frac{12l}{Ehb^3} \tag{7}$$

$$\gamma = \frac{f_{axial}l^2}{Ebh^3} \tag{8}$$

(2) - (8) come from analysis of the standard, constant cross section Euler-Bernoulli beam in which plane cross sections of the beam remain plane and deformations are sufficiently small to satisfy linear elasticity. These equations are very similar to the equations established in [6], but we have chosen to assume a plane stress condition for the flexure, ignoring the (1 - ν^2) stiffening factor due to the Poisson effect. The full derivation of these equations is beyond the scope of this work, but the interested reader is directed to [6] and [22]. (4) and (6) include the effects due to the action of an external axial force (in square brackets) on the flexure. This power series approximation comes from the solution for the axially loaded fixed-guided beam [22]. The force is applied in the local coordinate system, meaning it's line of

action is orthogonal to the end of the displaced beam. In (4) a tensile axial force serves to stiffen the flexure in the z direction, but increases the compliance about the y axis in (6). One principle for designing compliant mechanisms to perform well under compressive loads is inversion [5], or designing a mechanism such that load-bearing flexures are kept in tension. This compliance formulation enables the designer to include the role of these externally applied axial forces in the overall mechanism stiffness for a more accurate description of mechanism behavior under prescribed loading conditions.

B. Compliance Transformation

(1) - (8) describe the compliance properties of a single flexure, but the mechanisms in which we are interested are typically comprised of multiple flexures connecting sets of rigid links in both serial and parallel configurations. In order to analyze the stiffness properties of an entire mechanism, we must combine the flexure compliance matrix with knowledge of mechanism geometry to generate an equivalent *mechanism* compliance. This is achieved by first transforming the flexure compliance in the local coordinate frame into the output coordinate frame of the mechanism.

In general, for any system of springs, elements in parallel are those that experience the same displacement and their stiffnesses can therefore be added to create an equivalent stiffness. Elements in series experience the same load - their compliances add to create a single equivalent compliance. However, this combination is only possible when the stiffnesses or compliances to be added are expressed in a common coordinate system. Therefore, we require that the compliance matrix in (1) for each flexure in the mechanism be transformed to a common coordinate system.

This transformation refers the compliance of each flexure joint to the base coordinate system (usually attached to the output platform or link of a parallel mechanism), and, in general, will depend on the position and orientation of each flexure relative to the chosen base coordinate system. While the compliance matrix of each flexure explicitly represents a general six axis spring, the spatial transformation introduces the mechanism geometry into the computation of the overall compliance of the mechanism.

The 6x6 transformation of the flexure compliance into the base coordinate system can be decomposed into a rotation about the principal axes of the base coordinate system and a translation expressed in the base coordinate system.

$$\mathbf{T_{0/i}} = \begin{bmatrix} \mathbf{I} & \mathbf{0} \\ \mathbf{S(c_i - c_0)} & \mathbf{I} \end{bmatrix} \cdot \begin{bmatrix} \mathbf{R_{0/i}} & \mathbf{0} \\ \mathbf{0} & \mathbf{R_{0/i}} \end{bmatrix} \tag{9}$$

$\mathbf{I}$ is the 3x3 identity matrix, $\mathbf{R_i}$ is the orientation of the ith flexure hinge with respect to the base coordinate system, the vector $\mathbf{c_i - c_0}$ is the vector from the origin of the base coordinate system to the origin of the local flexure coordinate system, and $\mathbf{S(r)}$ is the cross product matrix with the following definition:

$$\mathbf{S(r)} = \begin{bmatrix} 0 & -r_z & r_y \\ r_z & 0 & -r_x \\ -r_y & r_x & 0 \end{bmatrix} \tag{10}$$

For each flexure in a parallel flexure mechanism the matrices $\mathbf{S}$ and $\mathbf{R}$ will be functions of the mechanism geometry. (9) can then be combined with the following relations

$$\mathbf{f_i} = \mathbf{K_i}\delta_\mathbf{i} \tag{11}$$

$$\mathbf{f_0} = \mathbf{K_0}\delta_\mathbf{0} \tag{12}$$

$$\delta_\mathbf{i} = \mathbf{C_i f_i} \tag{13}$$

$$\delta_\mathbf{0} = \mathbf{C_0 f_0} \tag{14}$$

to yield the result:

$$\mathbf{C_0} = \sum_i \mathbf{T_{0/i}}^{-\mathsf{T}} \mathbf{C_i} \mathbf{T_{0/i}}^{-1} \tag{15}$$

$$\mathbf{K_0} = \sum_i \mathbf{T_{0/i}} \mathbf{K_i} \mathbf{T_{0/i}}^{\mathsf{T}} \tag{16}$$

The property that $\mathbf{T_{0/i}^{-1}} = \mathbf{T_{i/0}}$ makes (15) and (16) equivalent to the transformation equations in [6].

III. Application to Compliant Mechanism Design

The application of the above formulation to compliant parallel mechanisms is motivated by our research in designing and building very small scale mobile robots, or millirobots. The enabling technology for design and fabrication of mobile millirobots like those in [17] and [11] is a design and fabrication paradigm known as Smart Composite Microstructures (SCM) [18]. The process integrates laser micromachined long fiber composites, with compliant polymer hinges and novel strain based actuators like piezoelectrics and shape memory alloys to create integrated, multi-DOF, articulated robotic structures. The SCM process for fabricating integrated flexural joints and rigid composite links is depicted in Fig. 2. From Fig. 2 we see that the SCM process is capable of producing only flat, constant cross section flexure hinges, thereby motivating our focus on this relatively simple geometry.

In addition to the constraints imposed by the limits of the SCM fabrication process, mobile millirobot design is highly constrained by the size and mass of the electronics and power source needed to power and control actuators. As such, past robot designs [20] [11] have made extensive use of parallel kinematics in order to appropriately couple and control the desired degrees of freedom while minimizing the number of required actuators.

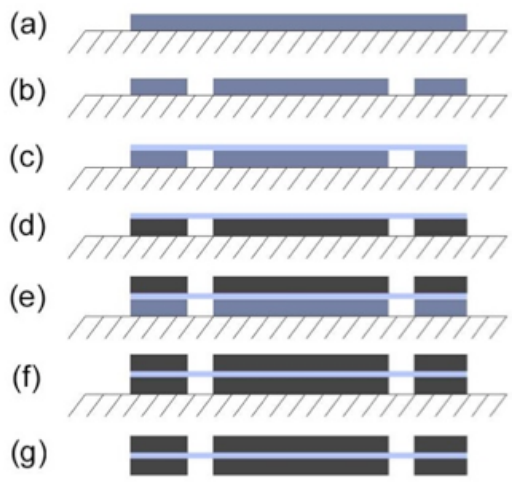

Fig. 2. The progression of the fabrication process for integrated, articulated, compliant microstructures. **a)** substrate of uncured pre-pregnated composite **b)** laser micromachining of gaps **c)** lamination of a thin polymer film **d)** curing of the composite layer bonds the polymer film **e)** alignment of the cured layer w/ polymer to an uncured layer with mirror symmetry **f)** curing of the entire structure bonds all layers **g)** compliant structure is released

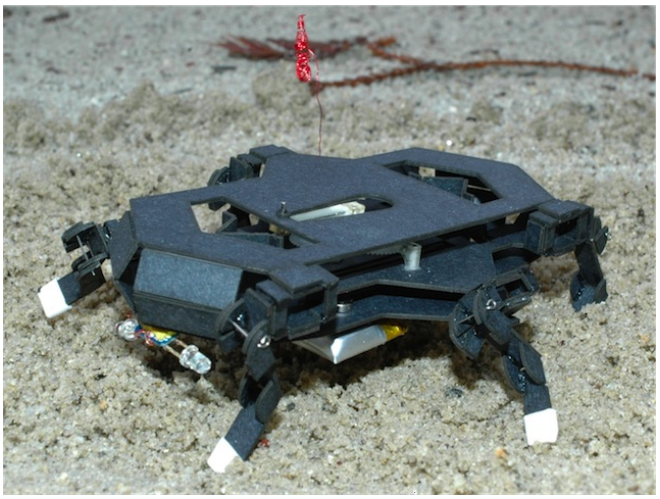

Fig. 3. A hexapedal robot fabricated using the SCM process. The central mechanism (hidden) connecting all six fourbar hips is a compliant Sarrus linkage.

A. A performance metric

With these considerations in mind, we aim to design a compliant mechanism that exhibits maximal compliance in the desired degrees of freedom and maximal stiffness in the undesired degrees of freedom. In order to compare the performance of different designs, it is therefore necessary to adopt a metric by which to judge a mechanism. In this work, we use the ratio of the so-called "mutual potential energy" [15] (also sometimes referred to as "mutual strain energy") to the total strain energy of the mechanism:

$$f = \frac{\text{MPE}}{\text{SE}} \tag{17}$$

The mutual potential energy is defined as:

$$\text{MPE} = \mathbf{v}^{\mathsf{T}}\mathbf{K}\mathbf{u} \tag{18}$$

where $\mathbf{v}$ is the displacement vector at the output when only a unit dummy load is applied in the desired output direction, $\mathbf{K}$ is the equivalent stiffness of the mechanism expressed in the base or output coordinate system, and $\mathbf{u}$ is the displacement vector when the entire input load is applied. Intuitively, we can think of mutual potential energy as the amount of useful work or displacement generated at the output port by an input load. The strain energy of the mechanism is given by:

$$\text{SE} = \frac{1}{2}\mathbf{u}^{\mathsf{T}}\mathbf{K}\mathbf{u} \tag{19}$$

Thus, the performance metric given in (17) is a ratio of the work output in the desired direction (the useful work) to the work done in deforming the mechanism. The larger this ratio, the more "efficient" the mechanism can be considered, ie. the undesirable degrees of freedom remain stiff while the desirable degrees of freedom are compliant.

B. Design Evaluation and Analysis

The application of this stiffness formulation and performance metric to compliant mechanisms fabricated using the SCM process is motivated by our interest in building, small, lightweight, mobile robots. These robots' highly constrained mechanical and kinematic requirements often lead to mechanically complex designs. For example, the hexapedal running robot in Fig. 3 possesses two degrees of freedom coupled through a single actuator as well as six unactuated degrees of freedom in the form of compliant knee joints. The mechanism kinematics and actuator configuration must appropriately couple the two controlled degrees of freedom to produce an alternating tripod gait.

As a simple example of the usefulness of modeling the full compliance of these SCM structures, we focus on the design of a mechanism that plays a prominent role in the robot pictured in Fig. 3, the Sarrus linkage. Fig. 4 shows a model of the robot in which a central Sarrus linkage (shown in blue) can been seen connecting two sets of three hips such that when it contracts the upper legs are adducted while the lower legs are abducted. The Sarrus' central role in this compliant robotic structure and the complex loads that are applied at the hips as a result of ground reaction forces transferred through the legs make it an interesting case study.

The most common (and minimal) topology of the Sarrus linkage (as pictured in Fig. 5) consists of two planar kinematic chains of 4 links connected by three hinges. The two chains are rigidly connected at their base and outputs and are oriented at an angle (usually 90°) with respect to each other such that the rotation axes of all the joints intersect. Mobility of the chain as predicted by Grübler's criterion is zero, so it's important that the rotation axes for the joints be precisely aligned.

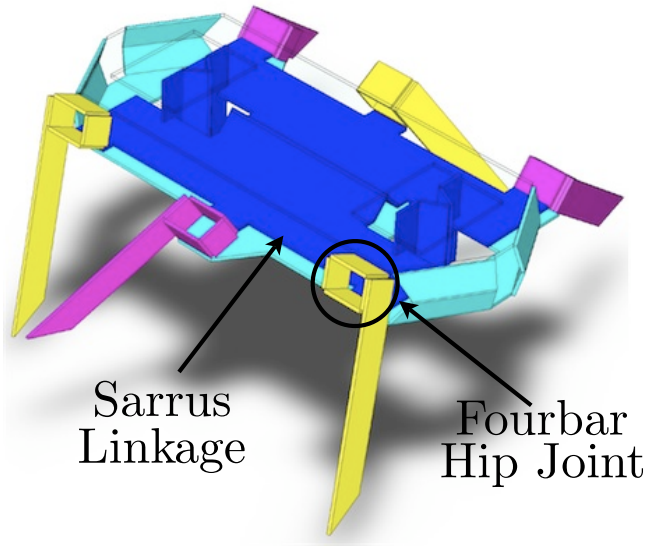

Fig. 4. A CAD model of a hexapedal crawler that uses a Sarrus linkage to connect six fourbar hip joints.

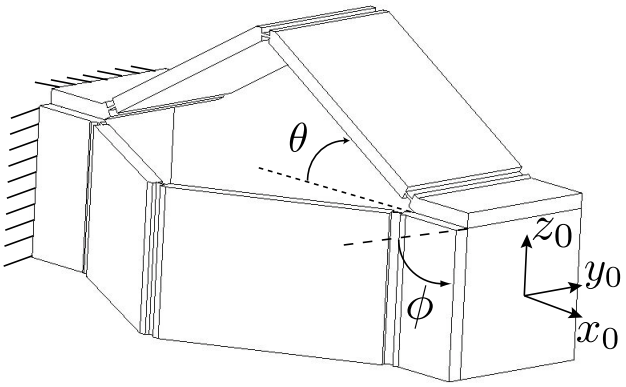

Fig. 5. A compliant Sarrus linkage shown with its simplest topology and configuration: Two 4 link kinematic chains rigidly joined at their base and output links and oriented at ϕ = 90°to each other.

Using conventional mechanical components, the Sarrus linkage would typically be constructed with pin-type hinges, which ideally provide infinite compliance in rotation about the hinge axis and infinite stiffness in all other directions. However, we are designing a compliant Sarrus linkage in which each hinge has finite compliance/stiffness. Given that fact, we are interested in the topologies and geometries of the Sarrus linkage which, for a given set of forces applied at the output, maximize the metric in (17).

The minimal topology for the compliant Sarrus consists of two serial kinematic chains connected at some angle, ϕ, with respect to each other. Conventional Sarrus linkage designs typically set ϕ = 90°. In fact, for conventional designs with ideal hinges, any angle other than zero and 180° will provide equivalent exact straight line motion constraint. However, for the compliant case, the angle between the two kinematic chains becomes an important design variable when considered in tandem with loading conditions at the output frame. All cases considered below have the geometric

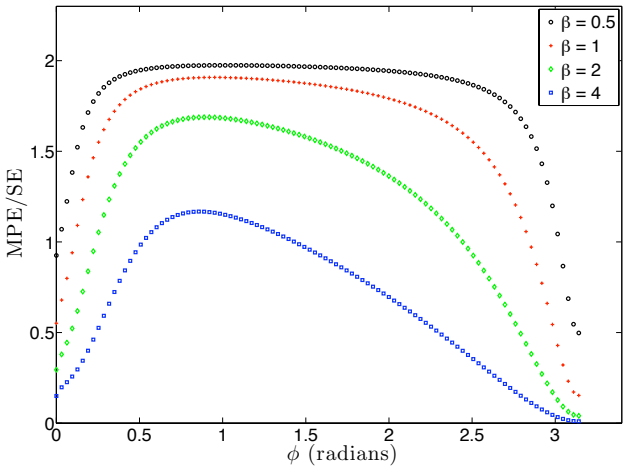

Fig. 6. Performance of a Sarrus linkage consisting of two kinematic chains connected at an angle, ϕ. The parameter β is the ratio of the off-axis forces to the force in the direction of highest compliance.

parameter θ (depicted in Fig. 5) set to 30°. Additionally, the loading condition considered is the simultaneous application of forces (but no moments) in all three axes. The β parameter represents the ratio of the magnitude of the two off-axis forces to the magnitude of the applied force in the compliant direction.

1) Case I: Two chain compliant Sarrus: This topology is shown in Fig. 5. We are interested in the angle between the two kinematic chains, ϕ that gives the best performance in the sense of (17) for forces in the x_0, y_0, z_0 coordinate frame. Fig. 6 shows the performance of the two chain Sarrus for the range $\phi \in [0, \pi]$ for four different loading conditions. The parameter β represents the ratio of the magnitude of the two off-axis forces (taken to be equal in these examples) to the forces in the direction of highest compliance (the x_0 direction, in this case).

From the figure, we see that as the off-axis forces become large in comparison to the force in the compliant direction, a clear optimal orientation angle for the kinematic chains appears at approximately 0.85 radians.

2) Case II: Three chain compliant Sarrus: From a strictly kinematic perspective, this redundancy is unnecessary for the straight line constraint. However, from a compliance perspective, our design intuition is that redundancy should provide an improvement in mechanism performance. Fig. 7 shows that, in fact, we do see an improvement in performance. For the case of relatively small off-axis forces (β=0.5) maximum performance is unchanged. However, the mechanism shows a reduced sensitivity to an increase in β at the optimal orientation angle of ϕ = 0.85 radians. It's important to note, however, that this relative insensitivity to off-axis forces only occurs at the optimal orientation angle. Away from that angle, performance drops markedly with increased off-axis loading. Additionally, the peak performance predicted for this configuration occurs to the left of the $\phi = \frac{\pi}{2}$ due to the asymmetric loading configuration. When the force

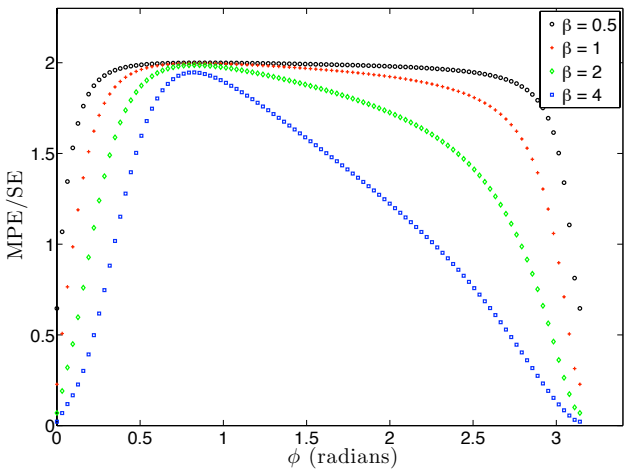

Fig. 7. Performance variation in a Sarrus linkage comprised of three kinematic chains with two chains connected at angles of ϕ and -ϕ with respect to the third. β is the ratio of off-axis forces to forces in the most compliant direction.

in the y direction is removed, because of the symmetry of the topology and geometry of the mechanism, the peak performance occurs at the angle $\phi = \frac{\pi}{2}$.

3) Case III: Four chain compliant Sarrus: The geometry of this case corresponds to a mirroring of the geometry in case I about the plane $z = y$. Results from the analysis of this topology are shown in Fig. 8.

This topology shows the best performance in two senses. First, the maximal performance is relatively insensitive to the orientation angle of the chains (away from the singular $\phi = 0$ and $\phi = \pi$ orientations). Secondly, the performance of the mechanism is relatively insensitive to increases in the off-axis loads over that range of ϕ.

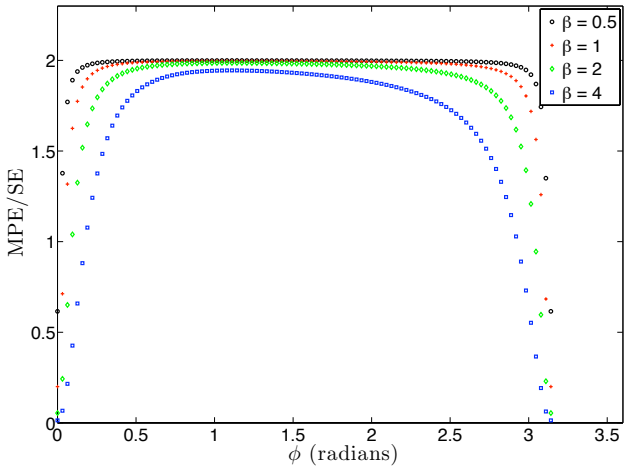

Fig. 8. Performance variation in a Sarrus linkage comprised of four kinematic chains. This configuration shows the overall best performance encapsulated by a lack of sensitivity to off-axis forces (β) as well as orientation angle (ϕ).

IV. Experimental Results

To test the predictions of model, we fabricated 5 different geometric configurations of two topologies of the Sarrus linkage - the two chain topology and the four chain topology. The mechanisms were constructed using the folding process

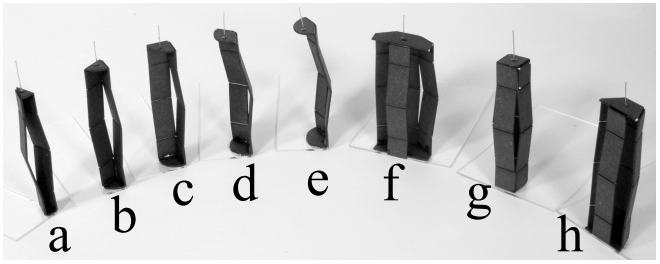

Fig. 9. Sarrus linkage topologies and configurations used to experimentally verify the predictions of the model. **a-e** are the five configurations of the two chain topology **a**, ϕ = 30° up to **e**, ϕ = 150°. **f-h** represent the five configurations for the four chain topology. For **f**, ϕ = 30°(150°), **g**, ϕ = 90°, and **h**, ϕ=60°(120°). Only three linkage configurations are necessary for the four chain topology because the 120° and 150° orientations are reflections of the 60° and 30° orientations respectively.

Parameter	Value
b	8mm
h	50μm
l	600μm
l_{link}	20mm
θ	10°

TABLE I
SARRUS LINKAGE GEOMETRIC PARAMETERS

described in [10]. Table I summarizes the common geometric parameters for all linkages tested.

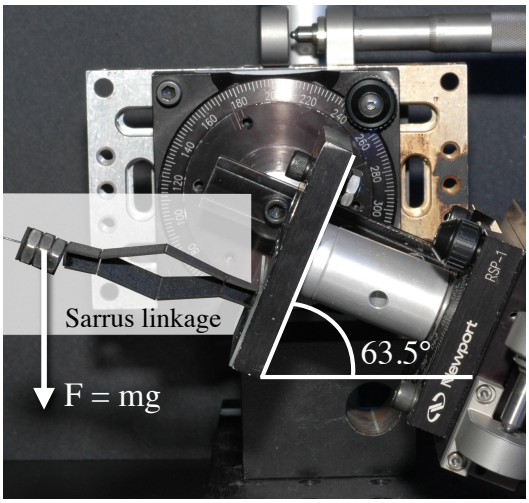

Fig. 10. Experimental setup used to generate controlled off-axis loading for testing compliant Sarrus linkage performance.

The base of each linkage was grounded and a load was applied to the output link at the free end by a simple mass as despicted in Fig. 10. The entire linkage was rotated through several angles to create ratios of off-axis to on-axis loading, β, of 0-2. The linear and angular displacements in the XZ plane were measured optically, and the 3x3 stiffness matrix was estimated from the displacement data using the procedure outlined in [2]. Results comparing the performance of the two topologies are shown in Fig. 11.

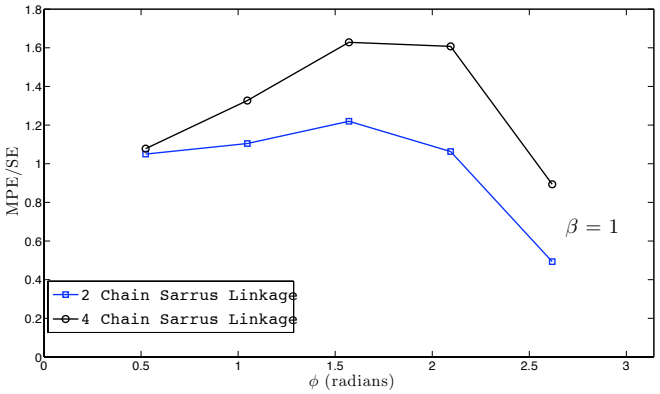

Fig. 11. Experimental measurement of the off-axis stiffness performance of two and four chain topologies of the compliant Sarrus linkage. For each topology 5 different configurations (orientation angles of the individual chains) were subjected to an off-axis force in the Z direction and a negative moment about the Y axis as well as an on-axis load in the negative X direction. The 4 chain Sarrus is preferable to the two chain topology and the peak performance, or maximal off-axis stiffness, for both occurs when the chains are oriented at $\frac{\pi}{2}$ radians or 90° to each other.

V. Conclusions and Discussion

By transforming the stiffnesses of simple, constant cross section, beam-like flexures into a common coordinate system we can generate an expression for the generalized stiffness of a compliant mechanism consisting of rigid links interconnected by flat flexures. Using a strain energy-based metric, we can analyze the performance of a given topology and geometry subject to a prescribed set of loads at the output of the mechanism. In this work, this approach has been applied to understanding and improving the off-axis performance of a compliant linkage commonly used in the design of our millirobots - the exact straight line Sarrus linkage.

Using the tools described we demonstrated a quantifiable improvement in the performance of the compliant Sarrus linkage by adjusting only the linkage topology. However, we have not optimized in any formal, global sense the topology or geometry of the mechanism. Rather, we have applied a straightforward closed form model to assist in understanding mechanism behavior under general loading conditions. That ability to quickly predict performance improvements of these compliant linkages has the potential to provide additional insights at the early stages of design and reduce the overall design cycle time for SCM millirobots.

It is important to note, however, that the results of this approach are dependent not only on the mechanism topology and geometry, but also on the loading conditions imposed at the output of the mechanism. This dependence of the mechanism performance on the loading condition requires the mechanism designer to understand the nature of the output loads associated with the intended application. If those loads are well understood, this approach provides a useful tool for guiding the initial exploration of the design space. Once a promising design has been identified, more intensive approaches such as finite element modeling can be applied to improve the precision or performance of the design.

References

[1] S. Awtar and A. Slocum, "Design of parallel kinematic xy mechanisms," in *Proceedings of the ASME International Design Engineering Technical Conferences*, vol. v 7 A. American Society of Mechanical Engineers, Sept. 2005, pp. 89–99.

[2] Y. Chen and J. McInroy, "Estimation of symmetric positive-definite matrices from imperfect measurements," *Automatic Control, IEEE Transactions on*, vol. 47, no. 10, pp. 1721–1725, Oct 2002.

[3] M. Culpepper and G. Anderson, "Design of a low-cost nano-manipulator which utilizes a monolithic, spatial compliant mechanism," *Precision Engineering*, vol. 28, no. 4, pp. 469–482, Oct. 2004.

[4] T. Ebefors, J. U. Mattsson, E. Kalvesten, and G. Stemme, "A walking silicon micro-robot," in *10th Intl Conf on Solid-State Sensors and Actuators*. IEEE, 1999, pp. 1202–1205.

[5] A. E. Guerinot, S. P. Magleby, L. L. Howell, and R. H. Todd, "Compliant joint design principles for high compressive load situations," *Journal of Mechanical Design*, vol. 127, no. 4, pp. 774–781, 2005. [Online]. Available: http://link.aip.org/link/?JMD/127/774/1

[6] L. C. Hale, "Principles and techniques for designing precision machines," Ph.D. dissertation, Massachusetts Institute of Technology, February 1999.

[7] L. C. Hale and A. H. Slocum, "Optimal design techniques for kinematic couplings," *Precision Engineering*, vol. 25, no. 2, pp. 114 – 127, 2001. [Online]. Available: http://www.sciencedirect.com/science/article/B6V4K-42MFF4X-5/2/2b1439cf4d7f883c918b2b415220df9d

[8] J. A. Hetrick, N. Kikuchi, and S. Kota, "Robustness of compliant mechanism topology optimization formulations," V. V. Varadan, Ed., vol. 3667, no. 1. SPIE, 1999, pp. 244–254. [Online]. Available: http://link.aip.org/link/?PSI/3667/244/1

[9] S. Hollar, A. Flynn, C. Bellew, and K. S. J. Pister, "Solar powered 10mg silicon robot," in *IEEE MEMS*, 2003.

[10] A. M. Hoover and R. S. Fearing, "Fast scale prototyping for folded millirobots," in *IEEE Int. Conf. on Robotics and Automation*, Pasadena, CA, 2008.

[11] A. M. Hoover, E. Steltz, and R. S. Fearing, "Roach: An autonomous 2.4g crawling hexapod robot," in *IEEE Int. Conf. on Intelligent Robots and Systems*, Nice, France, Sept. 2008.

[12] L. L. Howell, *Compliant mechanisms*. John Wiley & Sons, 2001.

[13] L. L. Howell and A. Midha, "A method for the design of compliant mechanisms with small-length flexural pivots," *Journal of Mechanical Design*, vol. 116, no. 1, pp. 280–290, 1994. [Online]. Available: http://link.aip.org/link/?JMD/116/280/1

[14] J. Selig and X. Ding, "A screw theory of static beams," *Intelligent Robots and Systems, 2001. Proceedings. 2001 IEEE/RSJ International Conference on*, vol. 1, pp. 312–317 vol.1, 2001.

[15] R. T. Shield and W. Prager, "Optimal structure design for given deflection," *Zeitschrift für Angewandte Mathematik und Physik (ZAMP)*, vol. 21, no. 4, pp. 513–523, July 1970.

[16] B. P. Trease, Y. Moon, and S. Kota, "Design of large displacement compliant joints," *Journal of Mechanical Design*, vol. 127, no. 4, pp. 788–798, July 2005.

[17] R. J. Wood, "The first takeoff of a biologically inspired at-scale robotic insect," *IEEE Trans. Robotics*, vol. 24, no. 2, pp. 341–347, April 2008.

[18] R. J. Wood, S. Avadhanula, R. Sahai, E. Steltz, and R. S. Fearing, "Microrobot design using fiber reinforced composites," *J. Mech. Design*, vol. 130, no. 5, May 2008.

[19] R. J. Wood, E. Steltz, and R. S. Fearing, "Optimal energy density piezoelectric bending actuators," *Sensors and Actuators*, vol. 119, pp. 476–488, 2005.

[20] J. Yan, S. A. Avadhanula, J. Birch, M. H. Dickinson, M. Sitti, T. Su, and R. S. Fearing, "Wing transmission for a micromechanical flying insect," *Journal of Micromechatronics*, vol. 1, pp. 221–237, 1 July 2001.

[21] L. Yin and G. K. Ananthasuresh, "Design of distributed compliant mechanisms," *Mechanics Based Design of Structures and Machines*, vol. 31, no. 2, pp. 151–179, 2003.

[22] W. C. Young and R. G. Budynas, *Roark's Formulas for Stress and Strain*, 7th ed. New York, NY: McGraw-Hill, 2001.